Physical Insights into Biological Memory using Phospholipid Membranes

Dima Bolmatov^{1,2*}, C. Patrick Collier^{3*}, John Katsaras^{1,2,4*} and Maxim O. Lavrentovich^{5*}

¹Department of Physics & Astronomy, University of Tennessee, Knoxville, 37996, Tennessee, United States.

²Shull Wollan Center, Oak Ridge National Laboratory, Oak Ridge, 37831, TN, United States.

³Center for Nanophase Materials Sciences, Oak Ridge National Laboratory, Oak Ridge, 37831, TN, United States.

⁴Neutron Scattering Division, Oak Ridge National Laboratory, Oak Ridge, 37831, TN, United States.

⁵Department of Earth, Environment, and Physics, Worcester State University, Worcester, 01602, Massachusetts, United States.

*Corresponding author(s). E-mail(s): dbolmato@utk.edu; colliercp@ornl.gov; katsarasj@ornl.gov; mlavrentovich@worcester.edu;

Abstract

Electrical signals may propagate along neuronal membranes in the brain, thus enabling communication between nerve cells. In doing so, lipid bilayers, fundamental scaffolds of all cell membranes, deform and restructure in response to such electrical activity. These changes impact the electromechanical properties of the membrane, which then physically store biological memory. This memory, can exist either over a short or long period of time. Traditionally, biological memory is defined by the strengthening or weakening of transmissions between individual neurons. Here, we show that electrical stimulation may also alter the properties of the lipid membrane, thus pointing toward a novel mechanism for memory storage. Furthermore, based on the analysis of existing electrophysiological data, we study molecular mechanisms underlying the long-term potentiation (LTP) in phospholipid membranes. Finally, we examine the relationship between the memory capacitive properties of lipid membranes, neuronal learning, and memory.

1 Introduction

Long-term potentiation (LTP) is a process observed in the brain and is associated with the strengthening of synaptic connections between neurons [1]. LTP is widely accepted as a fundamental mechanism responsible for neuronal learning and memory, and primarily takes place at synapses —i.e., the junctions between neurons [2]. When two neurons are connected, the presynaptic neuron releases neurotransmitters into the synaptic cleft that bind to receptors on the postsynaptic neuron, thus transmitting an electrical signal (see Figure 1). During LTP, repeated and persistent stimulation of the synapse leads to specific changes, such as the activation of certain types of glutamate receptors, primarily N-methyl-D-aspartate (NMDA), an excitatory neurotransmitter in the human brain [3]. The activation of these receptors allows for calcium ions to enter the postsynaptic neuron, triggering a cascade of intracellular processes that ultimately result in an increase in the number and sensitivity of the receptors populating the postsynaptic membrane [4]. This strengthening of synaptic connections leads to enhanced chemical signal transmission between the participating neurons and the formation of neural circuits associated with neuronal learning and memory, and information processing in the brain [5].

LTP and synaptic plasticity are two interconnected concepts that are crucial in understanding how the brain functions and the mechanisms underlying neuronal learning and memory [8]. As mentioned, synaptic plasticity is the ability of the membranous connections (synapses) between neurons in the brain to change in response to a modulated stimulus [9]. These molecular changes can either strengthen or weaken the connection between neurons—temporarily or permanently—depending on the nature and pattern of the mediated stimulation. Moreover, synaptic plasticity can either be short-term or long-term, depending on the duration of the changes [10]. Short-term synaptic plasticity, for example, typically involves temporary changes in synaptic strength that can last from seconds to minutes. These changes are often mediated by processes such as, presynaptic facilitation or depression, which modify the amount of neurotransmitter released from the presynaptic neuron. In contrast, long-term synaptic plasticity involves more sustained modifications in synaptic strength that can persist for hours, days, or even years. Long-term synaptic plasticity is thought to play a crucial role in learning, memory consolidation, and information storage in the brain [11].

Synaptic plasticity is now widely accepted as being the key mechanism that underpins learning and memory at the molecular and cellular levels in the human brain [7, 12]. Indeed, synaptic plasticity allows the brain to adapt to changing physicochemical conditions, namely changes to the release of neurotransmitters, neuromodulators, gene expression, intracellular signaling pathways, and modifications in the structure and function of the synapse, enabling the transmission and storage of information [13]. Therefore, both LTP and synaptic plasticity are dynamic processes that contribute to

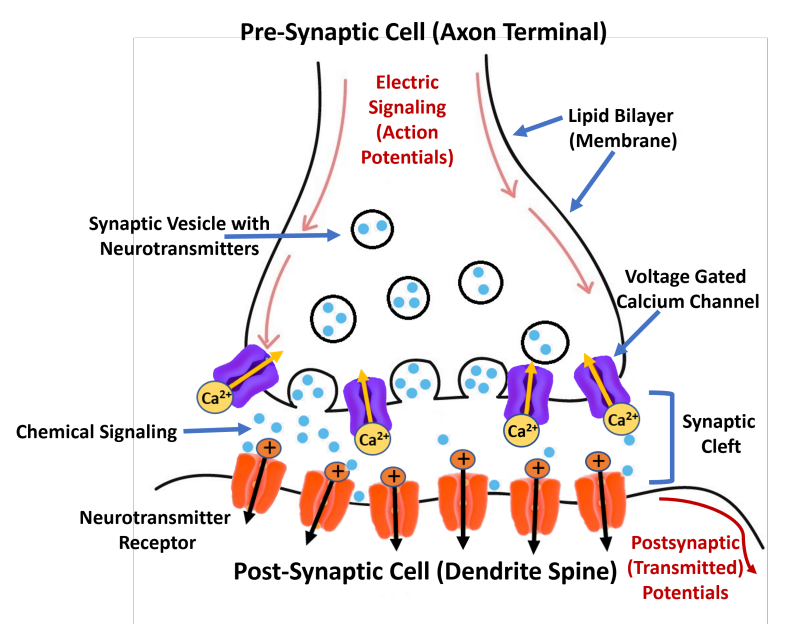


Fig. 1 Schematic representation of chemical signaling in a synapse. Synaptic plasticity can alter synaptic strength by either regulating the amount of neurotransmitter released into the synaptic gap from a presynaptic axon's membrane or by altering the number of postsynaptic receptors on a dendrite [6, 7].

the adaptability and flexibility of the brain. They allow the brain to modify its neural connections in response to new experiences and learning, ultimately shaping the brain's ability to remember and learn new information [14–16].

2 LTP in phospholipid membranes

While LTP is not a form of signal transmission in the conventional sense, it plays a crucial role in enhancing the strength of signal transmission between neurons at synapses [17]. We recently discovered that LTP in phospholipid membranes represents a new type of long-term synaptic plasticity [18, 19]. Specifically, LTP in phospholipid membranes emerges as a result of electrical stimulation of lipid bilayers in the absence of ion channels [18, 19]. Such electrical activity in lipid bilayers enables them to convert electric to mechanical energy repeatedly due to their piezoelectric and flexoelectric capabilities, with collective lipid motions playing a key role [20, 21]. In this manuscript, we explore molecular mechanisms underlying LTP in lipid membranes using different analytical models.

2.1 Memory elements and equivalent circuit models

A lipid bilayer is made up from two lipid monolayers, arranged tail-to-tail, with their headgroups immersed in water. The lipid bilayer is a key supramolecular structure

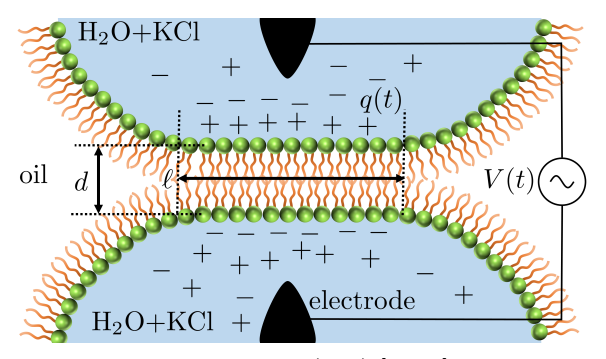


Fig. 2 Schematic of a droplet interface bilayer (DIB) [22–25]. To form it, two aqueous droplets immersed in oil (e.g., hexadecane) and decorated with a lipid monolayer (e.g., 1,2-diphytanoyl-sn-glycero-3-phosphocholine (DPhPC)), are brought together and a lipid bilayer of thickness d and diameter ℓ (surface area $A=\pi\ell^2/4$) is spontaneously formed. A sinusoidal voltage V(t) can be applied across the bilayer via two electrodes embedded in the water droplet, which can result in increasing charge asymmetry q(t) across the bilayer over time. Note that the solution's chemistry in each droplet is unaltered, even when there is charge asymmetry across the lipid bilayer.

of biological membranes, selective barriers separating a cell's intracellular and extracellular environments [26]. The chemical makeup of the lipid bilayer also make it an excellent insulator [27]. Thus, when an electric potential, V, is applied across it when immersed in an ionic solution, charge asymmetry, q(t), develops across the membrane —not unlike what takes place in a parallel plate capacitor [28, 29]. Fig. 2 shows a lipid bilayer of given diameter (ℓ) and thickness (d) formed by bringing together two lipid-decorated aqueous droplets immersed in an alkane hydrocarbon, where the lipid hydrocarbon acyl chains are interacting with the oil [30]. The presence of K^+ and Cl^- ions in the aqueous phase allows for q(t) to develop when a voltage, V(t), is applied across the electrodes —this is due to the difference in charge migration across the membrane for these two opositely charged ions. If we assume that these ions move through the solution with negligible impedance, then the amount of charge can be described by the lipid bilayer capacitance, C: q(t) = C(t)V(t). Let us consider this in greater detail.

Suppose we approximate the membrane as a parallel plate capacitor, with the lipid headgroup regions serving as "plates" and the lipid tails (i.e., the dielectric) sandwiched between them. Then, C is related to the membrane geometry via:

$$C = \frac{\epsilon_0 \epsilon A}{d},\tag{1}$$

where A is the membrane area (i.e., $A = \pi \ell^2/4$, shown in Fig. 2), q is the charge, d is the membrane thickness, ϵ is the relative dielectric constant of the membrane, and ϵ_0 is the vacuum permittivity. The parameters A, d, and ϵ may vary depending on the structure of the membrane and, in principle, can depend on the amounts of q or V, including their time-dependent histories. In such cases, the membrane can be conceptualized as a memory capacitor or memcapacitor with a time-dependent capacitance C(t).

A memcapacitor is a circuit memory element (memelement) with varying capacitance and obeys a set of equations given by [31]:

$$\begin{cases} q(t) = C(y, \{V, q\}, t)V(t) \\ \frac{dy}{dt} = f(y, \{V, q\}, t) \end{cases},$$

$$(2)$$

where memcapacitance, C, can depend on an auxiliary parameter, y, and either on q or V for charge- and voltage-controlled memcapacitors, respectively. y represents, for example, a change in membrane thickness when V is applied. To better illustrate this, we will use specific examples. Specifically, we will focus on the voltage-controlled case, where capacitance depends on y, which, in general, has dynamic properties that depend on V(t). For example, let us suppose that d in Eq. (1) varies linearly with y, so that $d(t) = d_0(1 + \alpha y)$, where the parameter α determines the strength of the thickness response to an applied voltage. In this case, we have:

$$C = \frac{C_0}{1 + \alpha y},\tag{3}$$

where $C_0 = \epsilon_0 \epsilon A/d_0$. In this case, A and d (Eq. (1)) of a DIB (Fig. 2) can also vary due to electrowetting and electrocompression induced by the voltage-dependent, in and out migration of the oil from bilayer [32]. Our simplified model can describe these changes, so long as the overall changes to C are captured by Eq. (3). It is important to note that more sophisticated models (see, e.g., Ref. [32]) can introduce dynamical equations to account for parameters such as, the membrane's thickness, d(t), and bilayer patch diameter, $\ell(t)$ (see Fig. 2). However, for simplicity, we will only consider d(t).

An interesting phenomenon is the response of a memcapacitor to an applied sinusoidal field, $V(t) = V_0 \sin(\omega t)$. The total work done by the voltage supply is given by $W = \int V \, \mathrm{d}q$. For a classical capacitor (assuming $\omega \ll (RC)^{-1}$ and neglecting dissipation from resistances R), after one cycle of the applied voltage, W equals zero, since the capacitor is charged and then discharged. In general, if the voltage supply transfers a specified amount of charge, q(t), into the system when transitioning from an initial voltage, V = 0, to a final voltage, V(t), at time t, then the total amount of work needed to move the charge can be written as:

$$W(t) = \int_0^{q(t)} V dq = \frac{[q(t)]^2}{2C(t)} + \frac{1}{2} \int_0^t V^2 \frac{dC}{dt} dt \equiv E_{\text{cap.}} + E_{\text{diss.}}, \tag{4}$$

describing the conservation of energy in the system. On the right hand side of the equation, the first term, $E_{\rm cap.}$, is the electrical energy stored in the capacitor due to the accumulated charge q(t). The second term, $E_{\rm diss.}$, only contributes when the capacitance, C(t) = q(t)/V(t), changes as a function of time. $E_{\rm diss.}$ represents the additional energy deposited or extracted from the system, which we will refer to as the dissipation energy —for reasons that will become obvious later on. For a classical capacitor with constant capacitance in the absence of any resistance, this term is always zero: i.e., $E_{\rm diss.} = 0$.

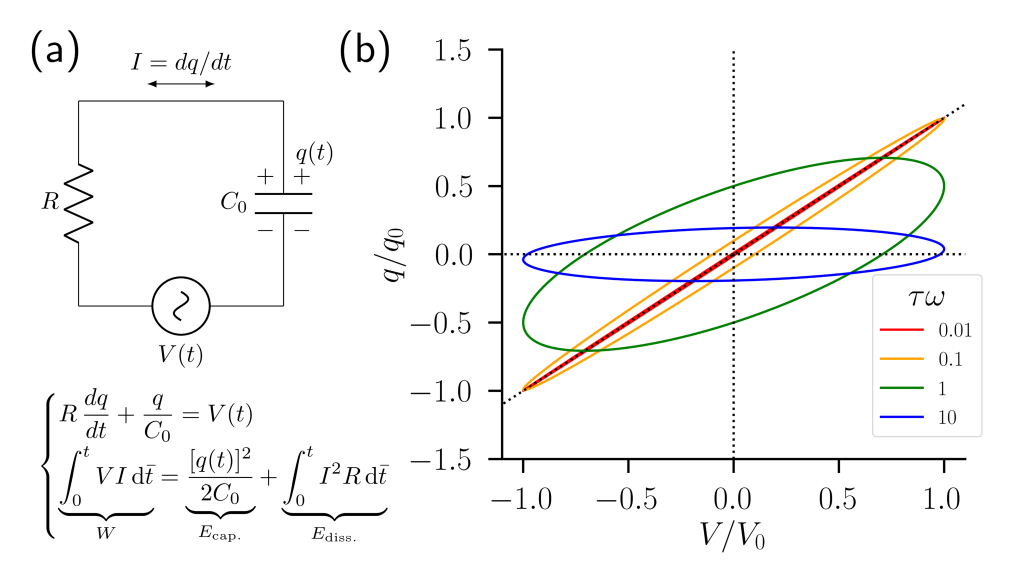


Fig. 3 (a) Schematic of an RC circuit driven by a sinusoidal applied voltage, $V(t) = V_0 \sin(\omega t)$. The first part of the equation shows the accumulated charge, q(t), at the capacitor according to Kirchhoff's laws, while the second line describes the energy conserved [33]. The work, W, supplied by the voltage source is used to both charge the capacitor (E_{cap}) and dissipate $(E_{\text{diss.}})$ the energy from the resistor. (b) A q-V response curve for the RC circuit shown in (a) for different values of the dimensionless quantity, $\tau \omega$, with $\tau = RC_0$ being the characteristic time of the circuit. Note that the hysteresis loop collapses into a line as $\tau \omega \to 0$.

A nontrivial value for $E_{\text{diss.}}$ emerges in the response of a circuit with a constant capacitance capacitor, C_0 , in series with a resistor of resistance, R (Fig. 3). In this circuit, $E_{\text{diss.}}$ represents the energy dissipated in the resistor since the quantity q(t)/V(t) varies with time due to the presence of the resistor. For a sinusoidal voltage, $V(t) = V_0 \sin(\omega t)$, the time dependence of the charge in the capacitor is given by:

$$q_{RC}(t) = \frac{C_0 V_0 \sin(\omega t)}{1 + \omega^2 C_0^2 R^2} \left[1 - \omega C_0 R \cot(\omega t) \right]. \tag{5}$$

In this case, the q-V response curve forms a single loop, as shown in Fig. 3(b). Over a single cycle, the work W supplied by the voltage source goes into the energy dissipated by the resistor, which can be written as:

$$W = \int_0^{2\pi/\omega} V \, \frac{dQ}{dt} \, dt$$

$$= E_{\text{diss.}} = \frac{1}{2} \int_0^{2\pi/\omega} V^2 \frac{dC}{dt} \, dt = \frac{\pi \tau \omega}{1 + \tau^2 \omega^2} \, C_0 V_0^2, \tag{6}$$

where $\tau \equiv RC_0$ is the characteristic time of the circuit. Here, we interpret the "time-dependent" capacitance as $C(t) \equiv q(t)/V(t)$. It is important to note, however, that the capacitor element itself retains a constant capacitance, C_0 . It is also important

to note that $E_{\text{diss.}}$ vanishes when the applied sine wave frequency ω is fast compared to τ (so that $E_{\text{diss.}} \to 0$ as $\tau \omega \to 0$). This occurs when the currents in the system become too small for resistive dissipation when the applied sinusoidal voltage form is significantly slower than the characteristic frequency, i.e., $\tau^{-1} = (RC_0)^{-1}$. In this low frequency regime, the q-V hysteresis loop collapses into a line (Fig. 3(b)).

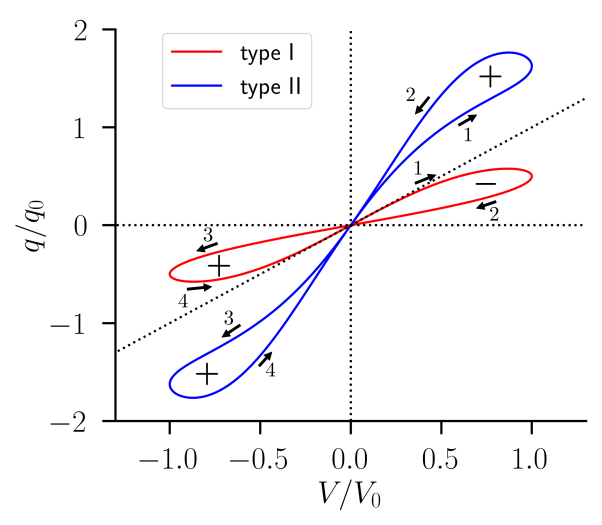


Fig. 4 Shown, are two types of memcapacitive behavior in response to an applied sinusoidal voltage, $V(t) = V_0 \sin(\omega t)$. The charge response is normalized by q_0 , with the response curves derived from specific examples described in the main text. Type I, also known as a passive response, does not require a net energy input from the voltage source. The energy input in the first half-period of the sine wave (paths 3 and 4) is completely returned during the second half (paths 1 and 2). On the other hand, the dissipative type II response requires a constant source of energy, as both half-cycles exhibit positive q-V loop areas.

For a memcapacitor, $E_{\rm diss.}$ can be non-zero due to an intrinsically time-dependent capacitance C(t). Unlike the RC model, dissipation can occur even in the absence of a resistor. Furthermore, the energy dissipation can be "negative", since memcapacitors can be active and contribute their own energy to the system. Even at sufficiently low frequencies, ω , where we can neglect resistive dissipation in the system through conduction, dq/dt, we can expect $E_{\rm diss.} \neq 0$ in Eq. (4). Moreover, in the absence of a phase lag due to a resistance, we expect the capacitance C = q/V (Eq. (2)) to be finite, as it will be determined by the physical parameters of the memcapacitor (as in Eq. (1)). Therefore, as $V \to 0$, we must have $q \to 0$, as well. This means that any q-V hysteresis loop must pass through the origin at q = V = 0 (i.e., it must have a pinch). This is because both q and V must approach zero at the pinch to maintain a finite C. At the pinch point, the hysteresis loops, known as type I and II, respectively (Fig.4).

In the case of a type I response hysteresis loop, there is no net energy input from the voltage source. Any energy input during the first half of the sine wave is returned in the second half. This type of self-crossing hysteresis loop is characteristic of most solid-state memcapacitors, and is often referred to as *passive* memcapacitance [34–36]. By contrast, for the dissipative type II response, the hysteresis loop does not self-cross, and each lobe requires the input of energy, which is then dissipated within the system [37]. This type of hysteresis loop is particularly relevant for biological membranes, which can, via their piezoelectric and flexoelectric properties [38], mechanically deform to dissipate the electrical energy into the surrounding aqueous solution [39–41].

We will now consider specific examples of type I and II hysteresis loop behavior, starting with the prototypical type I passive memcapacitor. Consider the following voltage-controlled memcapacitor, where the auxiliary parameter, y, obeys the equation of motion:

$$\dot{y} - V_0 \sin(\omega t) = 0, (7)$$

where the dot indicates a time derivative. In this case, capacitance simply tracks the integrated applied voltage and the accumulated charge accumulated for this type I memcapacitor is:

$$q_{\rm I}(t) = \frac{C_0 V_0 \sin(\omega t)}{1 + \overline{\alpha} [1 - \cos(\omega t)]},\tag{8}$$

where $\overline{\alpha} \equiv \frac{\alpha V_0}{\omega}$ is a dimensionless parameter that describes the strength of the memcapacitance. The result for $\overline{\alpha} = 1$ in appropriately re-scaled units (with $Q_0 \equiv C_0 V_0$) is shown by the red curve in Fig. 4. The released (paths 1 and 2) or introduced (paths 3 and 4) energies from the voltage source are given, for small $\overline{\alpha} \ll 1$, by

$$E_{\rm I} = \frac{2\overline{\alpha}}{3} C_0 V_0^2. \tag{9}$$

In the limit $\overline{\alpha} \to 0$, we recover the classical capacitor (with $E_{\rm I} \to 0$), where the curve in Fig. 4 evolves into a line with unit slope (dashed line). For any given value of $\bar{\alpha}$, there is no net energy inputted into the system over the full cycle of period $T = 2\pi/\omega$, so that $E_{\rm diss.} = 0$.

In contrast to a passive memcapacitor [42], a lipid membrane in an active memcapacitor can dissipate energy, similar to an RC circuit, leading to a non-zero $E_{\rm diss.}$. This dissipation comes, in part, from piezoelectric coupling, i.e., the conversion of electric to mechanical energy [43]. The energy conversion may generate, for instance, changes in membrane thickness and membrane area under an applied voltage, V. For the sake of simplicity, let us assume that these changes in membrane geometry can be described by a damped harmonic oscillator [44] i.e.:

$$\ddot{y} + \gamma \dot{y} + \omega_0^2 y + \beta V_0^2 \sin^2(\omega t) = 0, \tag{10}$$

where ω_0 is the characteristic oscillation frequency of the one degree of freedom, y, and γ is a damping coefficient. The term proportional to β is the electromechanical coupling [45], or the magnitude of the piezoelectric effect. Since this coupling should not depend on the sign of V, we can generally expect a quadratic dependence on the applied V(t) term. (In the case of a more detailed treatment, it is possible, for example, to introduce separate dynamical equations for membrane area, A, and thickness, d. Such an analysis was performed in Ref. [32], where parameters such as γ , ω_0 , and β were related to the electrowetting and electrocompression properties of the membrane.

In that case, the authors concluded that the dynamics of A and d were dominated by the damping term, so that the \ddot{y} term in Eq. (10) could be ignored. We will observe a similar behavior when we analyze the DIB data from Ref. [18].)

Combining Eq. (10) with Eq. (3) results in the capacitance dynamics of the system, given by:

 $C(t) = \frac{q_{\rm II}(t)}{V(t)} \approx \frac{C_0}{1 + \overline{\beta}^2 \operatorname{Re}\left[e^{2i\omega t}(1 + i\tau_{\gamma}\omega)^{-1} - 1\right]},\tag{11}$

where we now have the following key dimensionless parameters: the piezoelectric coupling strength $\overline{\beta}^2 \equiv \frac{\alpha\beta V_0^2}{2\omega_0^2}$ and a characteristic damping timescale $\tau_\gamma \equiv 2\gamma/\omega_0^2$. We also approximated that $\omega \ll \omega_0$ because we are interested in the low frequency (0.01 Hz) sinusoidal stimulation that was used in Ref. [18]. Taking all of this into account, we end up with the q-V response curve (blue) shown in Fig. 4, where $\tau_\gamma = 2$ sec and $\overline{\beta} = 1$. It is worth noting that both lobes of the hysteresis loop have positive areas, implying that the voltage source supplies energy for both half-periods of the voltage oscillation. Under this sufficiently slow drive (such that $\omega \ll \omega_0$), the approximate energy inputed into one sinusoidal cycle is given by:

$$E_{\rm II} \approx \frac{\overline{\beta}^2 (1 + 2\overline{\beta}^2)}{2} \left(\frac{\pi \tau_{\gamma} \omega}{1 + \tau_{\gamma}^2 \omega^2} \right) C_0 V_0^2. \tag{12}$$

We show similarities between an "elastic" memcapacitor and the RC circuit model by comparing the above equation (Eq. (12)) to Eq. (6). Note that while we can identify an effective "resistance" $R = \tau_{\gamma}/C_0$, the response of the memcapacitor is quite different in this case: we observe a pinched hysteresis, as shown in Fig. 4, instead of the RC circuit's elliptical hysteresis loop (Fig. 3(b)). Furthermore, the dissipated energy $E_{\rm II}$ does not necessarily manifest itself as heat, as one would expect in the RC circuit. Instead, there is the possibility that this energy is incorporated as changes to the memcapacitor itself. A detailed consideration of this specific case may provide a possible mechanism for LTP in lipid bilayers. We will now apply this elastic memcapacitor model to previously obtained experimental data from DIBs reported in Ref. [18].

2.2 Mechanisms for LTP formation in phospholipid bilayers

Recent work on DIBs [18] has shown that in the presence of a slow sinusoidal voltage waveform, a lipid membrane develops increased dissipative energy, $E_{\rm II}$. Although the mechanism of how this dissipative energy is formed is still not well-understood, we will use the elastic memcapacitor model to give us some insights into this recently observed phenomenon [18]. Using DPhPC DIBs in 500 mM KCl buffer solution and hexadecane, a voltage $V(t) = V_0 \sin(\omega t)$ was applied across the membrane, with $V_0 = 110$ mV and $f = \omega/2\pi = 0.01$ Hz. As discussed in Ref. [18], C(t) changed in the presence of the applied sinusoidal voltage waveform. The changes to the membrane were observed through the capacitive current response to a superimposed, high frequency triangle wave (frequency 10 Hz and amplitude 10 mV) —capacitance measurements are shown in Fig. 5(a). By fitting the parameters C_0 , τ_{γ} , and $\overline{\beta}$ to C(t) from Eq. (11), we are

able to recover the hysteretic behavior of the capacitance and gain some insights into the behavior of the membrane.

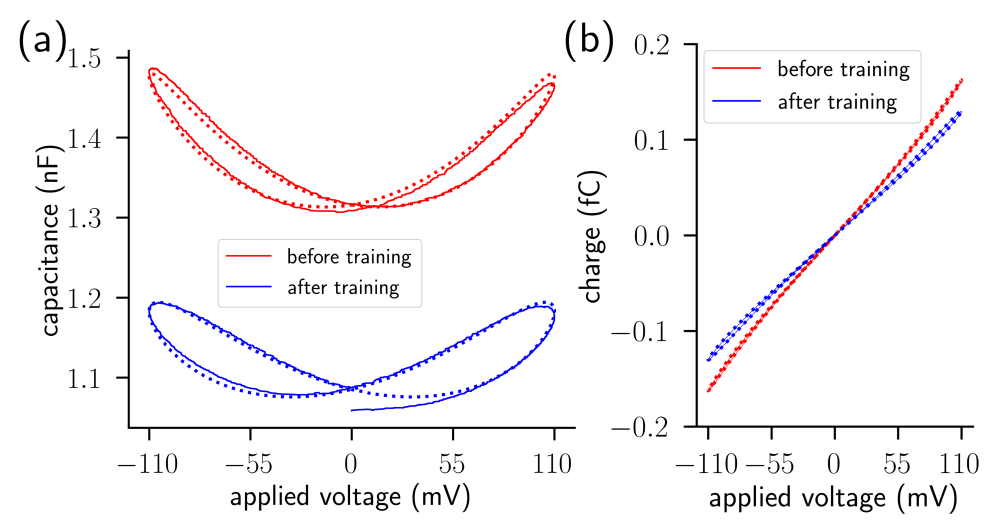


Fig. 5 The effect of training on capacitance or charge as a function of voltage. (a) The solid lines represent the time-dependent capacitance, C(t) = q(t)/V(t), as determined from experimental data in Ref. [18] for $V(t) = V_0 \sin(\omega t)$, with $V_0 = 110$ mV and $f = \omega/2\pi = 0.01$ Hz. The membrane after stimulation by a single sinusoidal voltage waveform is represented by the red curve. The blue curve is the capacitance hysteresis after a training period that included 36 sine waves and a subsequent waiting time of 200 minutes. The dashed lines are fits to the theoretical prediction in Eq. (11), as discussed in the main text. The sinusoidal voltage waveform training has two effects: (i) results in a decrease in the overall capacitance, C_0 , as evidenced by the lower position of the blue curve; and (ii) results in an increase in the dissipated energy as seen by the increased loop areas of the blue curve. (b) The capacitance curves in (a) may be used to calculate the q-V response curves via q = CV. We observe a decrease in slope of the curve after training and an increased hysteresis loop area. It is worth noting that the model (dashed lines) also captures the subtle non-linearities in the data (solid lines) at larges voltages.

In Ref. [18], the slow sinusoidal stimulation was applied for 36 cycles (60 minutes) before being switched off. Thereafter, the capacitive response to subsequent sine wave cycles was measured at increasing time intervals. The first sinusoidal voltage waveform (prior to training) and the last (taken about 200 minutes after training) are depicted by the red and blue curves, respectively, (Fig. 5(a)). The bare capacitance of the system varies around $C_0 \approx 1$ nF. Given a specific capacitance for DPhPC bilayers of 0.7 μ F/cm² [46], this corresponds to a lipid bilayer area of approximately 0.14 mm². After training, the capacitance drops by about 0.2 nF. There can be a few reasons for this drop. First, recent studies indicate that the relative permittivity ϵ near the membrane-water interface decreases due to the electric field stimulation [19]. This would decrease the capacitance, as can be seen from Eq. (1). Second, the membrane area might be decreasing under the stimulation, although this is likely a less important effect, as discussed in Ref. [19].

The capacitance C versus voltage V data (Fig. 5(a)) can be used to construct a Q vs V plot by setting Q = CV—this way we can compare it to the responses

discussed in the previous section. We see in Fig. 5(b) that the response shows a small hysteresis that is qualitatively the same as the type II hysteretic behavior shown in Fig. 4 (blue curve). Based on this, we expect that the elastic memcapacitor can serve as a reasonable model for the response of the membrane to an applied field. Note that, by construction, the measurement does not capture any resistive behavior because Q is calculated directly from a measurement of C.

We can now fit the capacitance measurements using Eq. (11). For the initial sine wave (red curve in Fig. 5(a)), we determined the following fitting parameters: $C_0 =$ 1.3106 ± 0.002 nF; $\tau_{\gamma} = 4.36 \pm 0.02$ sec; and $\beta = 0.2415 \pm 0.0002$ (with standard errors taken from the fit) —the fit is the red dashed line in Fig. 5(a). However, after training (blue curve), we obtained the following fitting parameters: $C_0 = 1.0640 \pm$ 0.0002 nF; $\tau_{\gamma} = 11.3 \pm 0.04 \text{ sec}$; and $\overline{\beta} = 0.2452 \pm 0.0003$. Note that the biggest differences between the before and after training data are a decrease in C_0 , by about 0.2 nF, and a significant (over 2-fold) increase in the damping parameter τ_{γ} . We have also estimated the characteristic frequency $-\omega$, by fitting to a model which does not assume $\omega \ll \omega_0$ —and found that $f_0 = \omega_0/2\pi \approx 2$ Hz, which is much larger than our stimulation frequency of 0.01 Hz (validating the $\omega \ll \omega_0$ approximation). Importantly, the large increase in τ_{γ} after training means that the membrane has a much larger dissipated energy $E_{\rm diss.}$. We should note that our model does not capture all of the dynamic features, such as the crossing of the red curve in Fig. 5(a) at a nonzero applied voltage, which can be the result of spontaneously-developed membrane charge asymmetry [47]. In addition, the experimental hysteresis curve (solid blue) is disconnected, as C_0 increases slightly over the course of stimulation by the sinusoidal voltage waveform.

The range of time scales, $\tau_{\gamma} \sim 4-11$ sec., arising from fits using the elastic memcapacitor model to the damping timescale τ_{γ} , is reminiscent of the relaxation of lipid membrane elastic fluctuations. For example, slow undulation modes in fluid membranes can be described by the hydrodynamic dispersion relation $\omega \approx \kappa q^3/2\eta$ [48]. With $\eta \approx 10^{-3}$ Pa · sec (i.e., the viscosity of water) and $\kappa \approx 1.2 \times 10^{-19}$ J for the DPhPC bending modulus [49], we find $f = \omega/2\pi = 0.01-10$ Hz for undulations with length scales between 0.01 mm $< \lambda < 0.1$ mm. Earlier work on a similar system [32] found similar timescales for electrostriction and electrowetting due to the oil in the DIB systems. Thus, these effects most likely, also contribute to the values of the memcapacitor model parameters. Regardless, it is clear that electrical stimulation excites slow mechanical modes, which, in turn, alter membrane structure. These changes to the membrane may then help explain the observed long-lived enhancement (after training) of the dissipated energy observed in Ref. [18].

A more complete picture of what takes place during the training and subsequent "LTP" phase emerges by using the elastic memcapacitor model to fit experimental data for all time periods of sine wave stimulation. The changes in the membrane under voltage stimulation are captured by just two parameters: i.e., the damping timescale, $\tau_{\gamma} = \gamma/\omega_0^2$, and the "bare" capacitance, C_0 (the capacitance at zero auxiliary parameter y = 0). We find that the training procedure essentially "trades off" capacitance (smaller C_0) for increased damping (larger τ_{γ}). The results are shown in Fig. 6 (a). After the initial training period (dotted black line), τ_{γ} saturates to a large value,

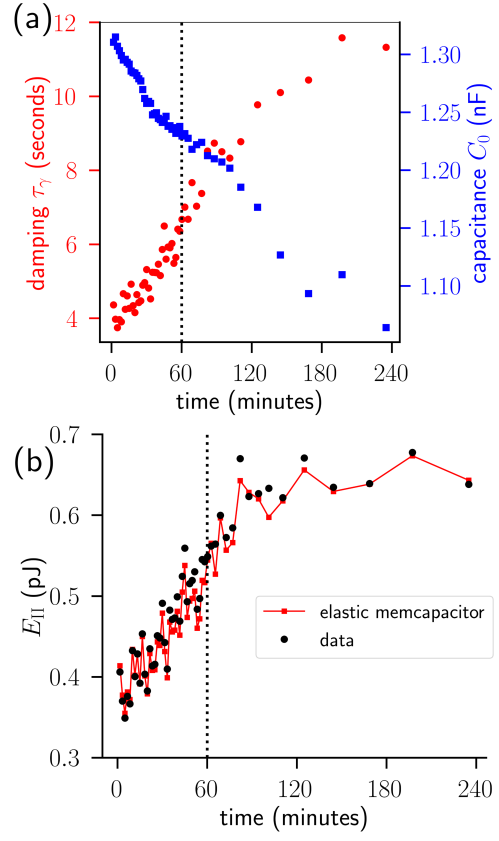


Fig. 6 (a) Fits to data from Ref. [18] using the elastic memcapacitor model. For the first 60 minutes (up to the vertical dotted line), the system was stimulated with a continuous sine wave. Thereafter, the applied voltage was turned off and single periods of the sine wave were applied at the indicated points. Note that the damping parameter, τ_{γ} , increases due to the stimulation, while the bare capacitance, C_0 , decreases. (b) We can calculate the energy dissipated in the system, $E_{\rm II}$, using both the data (black points) and the values from the fits to the data using the elastic memcapacitor model (see Eq. (12)). The dissipated energy increases during the training period and then plateaus. As discussed in Ref. [18], this plateau is long-lived (lasting for hours) and is a hallmark of the LTP phase. Note that the model captures the behavior of the dissipated energy.

while C_0 plateaus at a lower value. These values persist over many hours, with the membrane returning to its original, unperturbed state, after about 24 hours [18].

It is worth noting that the damping time constant τ found here (Fig. 6(a)) is about an order of magnitude larger than the damping timescale found due to electrowetting [32]. Thus, there are likely other processes, such as the organization of the cations [19] at the membrane interface, that contribute to these dynamics. Of course, electrowetting should still contribute to the τ parameter and it would be interesting to disentangle the various effects that contribute to both the long and short relaxation timescales found for these stimulated membranes. Finally, note that the strength of the piezoelectric effect $(\bar{\beta})$ does not vary much under the stimulation: We find a

mean value of $\langle \overline{\beta} \rangle = 0.341$ with a very small standard deviation $\sigma_{\overline{\beta}} = 0.002$ over all stimulation conditions shown in Fig. 6.

3 Discussion and Conclusions

Based on the analysis of existing experimental data, we have shown how membranes can deform and change their capacitive properties under electrical stimulation. We have analyzed these changes and their electrophysiological response using the elastic memcapacitor model that captures the hysteretic behavior of the charge versus voltage membrane response. By fitting experimental data to the model, we identify a key time scale $\tau_{\gamma} \sim 5-10$ sec corresponding to the dissipative modes in the system. We show that the increase in energy dissipation and long-lived changes in the hysteresis loops, under prolonged sinusoidal stimulation of the membrane, can be captured by just two parameters namely, a decrease in the zero-bias capacitance, C_0 , and an increase in the damping parameter, τ_{γ} .

The framework presented here may be useful for understanding the response of biological membranes in a neuronal context. Electrical signalling between neutrons occurs on timescales of up to hundreds of milliseconds and voltage changes similar to the ones analyzed in this report. Such signalling is typically analyzed in the context of neutrotransmitter dynamics and other synaptic transmission. Traditionally, biological memory is defined by the strengthening or weakening of these transmissions between individual neurons. However, our work shows that electrical stimulation may also alter the properties of the lipid membrane of the neuron, thus pointing toward a novel mechanism for memory storage.

In the present study, we explored electrical stimulation at a relatively low frequency (0.01 Hz) and identified sustained alterations in membrane properties over an extended period (several hours). It remains to be determined whether similar enduring changes can be observed under faster electrical stimulations, which may induce additional and faster relaxation modes. In future experiments, our goal is to investigate the memory effects induced in phospholipid membranes by continuous brain wave patterns, including α -, β -, and γ -waves, as well as electrical activities characterized by millisecond-scale spikes and bursts, among other factors.

Acknowledgments. It is our great pleasure and honor to dedicate this paper to our friend and colleague Professor Fyl Pincus. Fyl's prodigious scientific contributions to theoretical soft condensed matter physics continue to inspire us all. D.B. and M.L. are supported through the National Science Foundation, Division of Molecular and Cellular Biosciences (MCB), under contract no. 2219289. J.K. and C.P.C. are supported through the Scientific User Facilities Division of the Department of Energy (DOE) Office of Science, sponsored by the Basic Energy Science (BES) Program, DOE Office of Science, under Contract No. DEAC05-00OR22725. Some of the analysis was performed at the Center for Nanophase Materials Sciences, a US DOE Office of Science User Facility.

Authors's contribution

All authors contributed equally.

Funding. D.B. and M.L. are supported through the National Science Foundation, Division of Molecular and Cellular Biosciences (MCB), under contract no. 2219289.

Data availability statement. Data will be made available on reasonable request.

References

- [1] Bliss, T.V., Collingridge, G.L.: A synaptic model of memory: long-term potentiation in the hippocampus. Nature **361**(6407), 31–39 (1993)
- [2] Lømo, T.: The discovery of long-term potentiation. Trans. R. Soc. Lond., B, Biol. Sci. 358(1432), 617–620 (2003)
- [3] Collingridge, G.L., Bliss, T.: Nmda receptors-their role in long-term potentiation. Trends Neurosci. **10**(7), 288–293 (1987)
- [4] Nicoll, R.A.: A brief history of long-term potentiation. neuron **93**(2), 281–290 (2017)
- [5] Jackman, S.L., Regehr, W.G.: The mechanisms and functions of synaptic facilitation. Neuron **94**(3), 447–464 (2017)
- [6] Südhof, T.C.: Towards an understanding of synapse formation. Neuron 100(2), 276–293 (2018)
- [7] Vardi, R., Tugendhaft, Y., Kanter, I.: Neuronal plasticity features are independent of neuronal holding membrane potential. Physica A: Statistical Mechanics and its Applications **632**, 129351 (2023)
- [8] Jiang, F., Bello, S.T., Gao, Q., Lai, Y., Li, X., He, L.: Advances in the electrophysiological recordings of long-term potentiation. Int. J. Mol. Sci. 24(8), 7134 (2023)
- [9] Morris, R.G.: Long-term potentiation and memory. Trans. R. Soc. Lond., B, Biol. Sci. 358(1432), 643–647 (2003)
- [10] Abbott, L.F., Nelson, S.B.: Synaptic plasticity: taming the beast. Nat. Neurosci. **3**(11), 1178–1183 (2000)
- [11] Lüscher, C., Nicoll, R.A., Malenka, R.C., Muller, D.: Synaptic plasticity and dynamic modulation of the postsynaptic membrane. Nat. Neurosci. **3**(6), 545–550 (2000)
- [12] Magee, J.C., Grienberger, C.: Synaptic plasticity forms and functions. Annu. Rev. Neurosci. 43, 95–117 (2020)

- [13] Abarbanel, H.D., Huerta, R., Rabinovich, M.: Dynamical model of long-term synaptic plasticity. Proc. Natl. Acad. Sci. U.S.A. 99(15), 10132–10137 (2002)
- [14] Ma, S., Zuo, Y.: Synaptic modifications in learning and memory—a dendritic spine story. In: Seminars in Cell & Developmental Biology, vol. 125, pp. 84–90 (2022). Elsevier
- [15] Rouleau, N., Levin, M.: The multiple realizability of sentience in living systems and beyond. Eneuro **10**(11) (2023)
- [16] Bernard, C.: Brain Mysteries: Complexity beyond Imagination. Society for Neuroscience (2023)
- [17] Ma, X., Xu, Y.: Taming the hybrid synapse under energy balance between neurons. Chaos, Solitons & Fractals 159, 112149 (2022)
- [18] Scott, H.L., Bolmatov, D., Podar, P.T., Liu, Z., Kinnun, J.J., Doughty, B., Lydic, R., Sacci, R.L., Collier, C.P., Katsaras, J.: Evidence for long-term potentiation in phospholipid membranes. Proc. Natl. Acad. Sci. U.S.A. 119, 2212195119 (2022)
- [19] Scott, H.L., Bolmatov, D., Premadasa, U.I., Doughty, B., Carrillo, J.-M.Y., Sacci, R.L., Lavrentovich, M., Katsaras, J., Collier, C.P.: Cations control lipid bilayer memcapacitance associated with long-term potentiation. ACS Appl. Mater. Interfaces 15(37), 44533–44540 (2023)
- [20] Bolmatov, D., Collier, C.P., Zav'yalov, D., Egami, T., Katsaras, J.: Real space and time imaging of collective headgroup dipole motions in zwitterionic lipid bilayers. Membranes **13**(4), 442 (2023)
- [21] Bolmatov, D.: The phonon theory of liquids and biological fluids: Developments and applications. J. Phys. Chem. Lett. **13**(31), 7121–7129 (2022)
- [22] El-Beyrouthy, J., Freeman, E.: Characterizing the structure and interactions of model lipid membranes using electrophysiology. Membranes 11(5), 319 (2021)
- [23] Haylock, S., Friddin, M.S., Hindley, J.W., Rodriguez, E., Charalambous, K., Booth, P.J., Barter, L.M., Ces, O.: Membrane protein mediated bilayer communication in networks of droplet interface bilayers. Commun. Chem. 3(1), 77 (2020)
- [24] Huang, Y., Fuller, G., Suja, V.C.: Physicochemical characteristics of droplet interface bilayers. Adv. Colloid Interface Sci. 304, 102666 (2022)
- [25] Baxani, D., Jamieson, W., Barrow, D., Castell, O.: Encapsulated droplet interface bilayers as a platform for high-throughput membrane studies. Soft Matter 18(27), 5089–5096 (2022)
- [26] Bolmatov, D., Soloviov, D., Zhernenkov, M., Zav'yalov, D., Mamontov, E.,

- Suvorov, A., Cai, Y.Q., Katsaras, J.: Molecular picture of the transient nature of lipid rafts. Langmuir **36**(18), 4887–4896 (2020)
- [27] Hodgkin, A.L., Huxley, A.F.: A quantitative description of membrane current and its application to conduction and excitation in nerve. Physiol. J. 117(4), 500 (1952)
- [28] Smirnova, E.Y., Anosov, A.A.: Bilayer lipid membrane as memcapacitance: Capacitance-voltage pinched hysteresis and negative insertion conductance. Membranes 13(1), 97 (2023)
- [29] Ermakov, Y.A.: Electric fields at the lipid membrane interface. Membranes 13(11), 883 (2023)
- [30] Sacci, R.L., Scott, H.L., Liu, Z., Bolmatov, D., Doughty, B., Katsaras, J., Collier, C.P.: Disentangling memristive and memcapacitive effects in droplet interface bilayers using dynamic impedance spectroscopy. Adv. Electron. Mater. 8(5), 2200121 (2022)
- [31] Chen, B., Xu, Q., Chen, M., Wu, H., Bao, B.: Initial-condition-switched boosting extreme multistability and mechanism analysis in a memcapacitive oscillator. Front. Inf. Technol. Electron. Eng. **22**(11), 1517–1531 (2021)
- [32] Najem, J.S., Hasan, M.S., Williams, R.S., Weiss, R.J., Rose, G.S., Taylor, G.J., Sarles, S.A., Collier, C.P.: Dynamical nonlinear memory capacitance in biomimetic membranes. Nat. Commun. 10, 3239 (2019)
- [33] Demasius, K.-U., Kirschen, A., Parkin, S.: Energy-efficient memcapacitor devices for neuromorphic computing. Nat. Electron. 4(10), 748–756 (2021)
- [34] Strukov, D.B., Snider, G.S., Stewart, D.R., Williams, R.S.: The missing memristor found. nature 453(7191), 80–83 (2008)
- [35] Radwan, A.G., Fouda, M.E.: Memcapacitor: Modeling, Analysis, and Emulators, pp. 151–185. Springer, Cham (2015)
- [36] Romero, F.J., Ohata, A., Toral-Lopez, A., Godoy, A., Morales, D.P., Rodriguez, N.: Memcapacitor and meminductor circuit emulators: A review. Electronics 10(11), 1225 (2021)
- [37] Ball, P.: Soft learning. Nat. Mater. **22**(1), 2–2 (2023)
- [38] Jákli, A., Harden, J., Bailey, C.: Piezoelectricity of phospholipids: a possible mechanism for mechanoreception and magnetoreception in biology. Liquid Crystals 35, 395–400 (2008)
- [39] Bolmatov, D., Cai, Y.Q., Zav'yalov, D., Zhernenkov, M.: Crossover from picosecond collective to single particle dynamics defines the mechanism of lateral

- lipid diffusion. Biochimica et Biophysica Acta (BBA)-Biomembranes **1860**(11), 2446–2455 (2018)
- [40] Bolmatov, D., Zhernenkov, M., Zav'yalov, D., Stoupin, S., Cai, Y.Q., Cunsolo, A.: Revealing the mechanism of the viscous-to-elastic crossover in liquids. J. Phys. Chem. Lett. 6(15), 3048–3053 (2015)
- [41] Bolmatov, D., Zhernenkov, M., Zav'yalov, D., Stoupin, S., Cunsolo, A., Cai, Y.Q.: Thermally triggered phononic gaps in liquids at thz scale. Sci. Rep. 6(1), 19469 (2016)
- [42] Zhao, L., Fan, Z., Cheng, S., Hong, L., Li, Y., Tian, G., Chen, D., Hou, Z., Qin, M., Zeng, M., et al.: An artificial optoelectronic synapse based on a photoelectric memcapacitor. Adv. Electron. Mater. 6(2), 1900858 (2020)
- [43] Harden, J., Diorio, N., Petrov, A.G., Jakli, A.: Chirality of lipids makes fluid lamellar phases piezoelectric. Phys. Rev. E **79**(1), 011701 (2009)
- [44] Pershin, Y.V., Ventra, M.D.: Memory effects in complex materials and nanoscale systems. Adv. Phys. **60**(2), 145–227 (2011)
- [45] Mosgaard, L.D., Zecchi, K.A., Heimburg, T.: Mechano-capacitive properties of polarized membranes. Soft Matter 11, 7899 (2015)
- [46] Taylor, G.J., Venkatesan, G.A., Collier, C.P., Sarles, S.A.: Direct in situ measurement of specific capacitance, monolayer tension, and bilayer tension in a droplet interface bilayer. Soft Matter 11, 7592–7605 (2015)
- [47] Schoch, P., Sargent, D.F., Schwyzer, R.: Capacitance and conductance as tools for the measurement of asymmetric surface potentials and energy barriers of lipid bilayer membranes. J. Membrane Biol. 46, 71–89 (1979)
- [48] Brochard, F., Lennon, J.F.: Frequency spectrum of the flicker phenomenon in erythrocytes. J. Phys. (Paris) **36**, 1035–1047 (1975)
- [49] Karamdad, K., Law, R.V., Seddon, J.M., Brooks, N.J., Ces, O.: Preparation and mechanical characterisation of giant unilamellar vesicles by a microfluidic method. Lab Chip 15, 557–562 (2015)
- [50] Virtanen, P., Gommers, R., Oliphant, T.E., Haberland, M., Reddy, T., Cournapeau, D., Burovski, E., Peterson, P., Weckesser, W., Bright, J., van der Walt, S.J., Brett, M., Wilson, J., Millman, K.J., Mayorov, N., Nelson, A.R.J., Jones, E., Kern, R., Larson, E., Carey, C.J., Polat, İ., Feng, Y., Moore, E.W., Vander-Plas, J., Laxalde, D., Perktold, J., Cimrman, R., Henriksen, I., Quintero, E.A., Harris, C.R., Archibald, A.M., Ribeiro, A.H., Pedregosa, F., van Mulbregt, P., SciPy 1.0 Contributors: SciPy 1.0: Fundamental Algorithms for Scientific Computing in Python. Nature Methods 17, 261–272 (2020) https://doi.org/10.1038/

Appendix: Data analysis

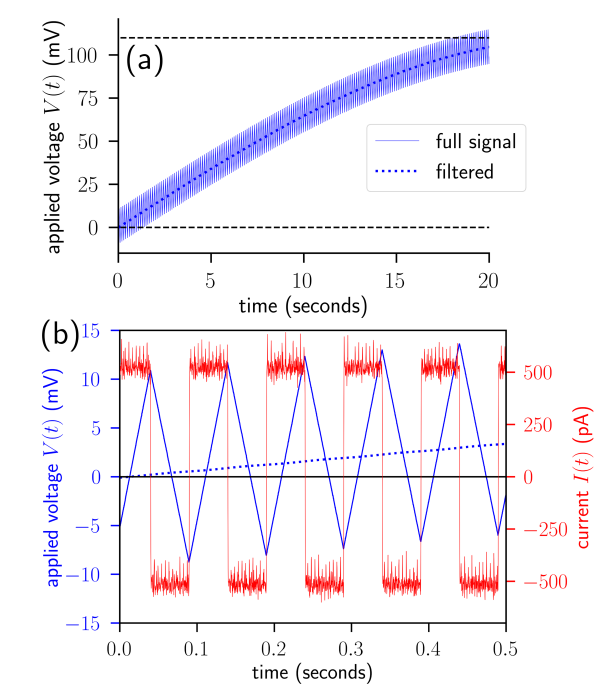


Fig. 7 (a) The blue line shows a portion of the applied voltage signal from voltage patch clamp experiments on DIBs from Ref. [18]. The signal consists of a superposition of a 0.01 Hz sine wave (with amplitude 110 mV, indicated by the upper black dashed line) and a 10 mV triangle wave at 10 Hz. We applied a filter to this data (thicker dotted line) that removes the triangle wave, as described in the main text. (b) Zooming in shows the full signal with the solid blue line and the filtered signal with the blue dotted line. We also see the raw measured current (provided by the authors of Ref. [18]), due to the applied voltage (red curve). The current switches sign according to the direction of the voltage ramp of the triangle wave. This capacitive current was used to calculate the membrane capacitance.

We used the raw electro-physiological DIB data provided by the authors of Ref. [18]. For the purposes of this manuscript, the relevant information is that a single lipid bilayer was stimulated under voltage clamp conditions, wherein a specified voltage, V(t), was applied across the membrane over time. The applied voltage consisted of a superposition of a slowly-varying sine wave and a triangle wave: $V(t) = V_0 \sin(2\pi t/T_0) + V_t \left[\left| 4\left((t-T_t/4) \mod T_t\right)/T_t - 2\right| - 1 \right]$, where the amplitude of the sine wave was $V_0 = 110$ mV and $V_t = 10$ mV for the triangle wave. The periods were $T_0 = 100$ sec and $T_t = 0.1$ sec for the sine and triangle waves, respectively.

We used the triangle wave to calculate the "instantaneous" capacitance C(t) of the membrane. The triangle wave probe was then stripped from the voltage signal to determine the capacitance response to sinusoidal stimulation. This was done by

first filtering the voltage signal through a Butterworth bandpass filter (from the scipy package in Python [50]) between 0.5 and 500 Hz. This isolated the triangle wave, which was then subtracted from the total signal. The resultant voltage signal was then passed through a low-pass filter with a cutoff frequency of 5 Hz. This eliminated any residual high frequency noise resulting from the subtraction process and from the voltage supply. An example of the fully-processed voltage signal is shown in Fig. 7(a) (thick dotted line), along with the raw voltage signal V(t) (thin solid line).

The capacitance C(t) can be read off from the triangle wave because the voltage ramps generate capacitive currents (Fig. 7(b)). The current response (red curve) is approximately constant during the linear voltage ramps of the triangle wave, so that $Q(t) \approx \langle I(t) \rangle t$ over the linear ramp segments, where $\langle I(t) \rangle$ represents the average current over the voltage ramps, for which $V(t) \approx \alpha_V t$ for a constant α_V . Assuming that the capacitance, C, is approximately constant over 0.1 seconds and that the triangle wave amplitude is small enough as to not induce leakage currents or other changes to C, then we have $I(t) = \frac{dQ}{dt} \approx C\frac{dV}{dt}$. Therefore, capacitance can be calculated directly from the measured current over each voltage ramp in the triangle wave: We averaged over each ramp, yielding an estimate $C(t) \approx \langle I(t) \rangle / \alpha_V$, where $\alpha_V = 400 \text{ mV/sec}$ is the slope of the triangle wave and we averaged the current I(t) over each voltage ramp "plateau" (see red curve in Fig. 7(b)). In order to eliminate the signal from the regions where the voltage ramps change signs, we only averaged over currents satisfying |I(t)| > 100 pA. Finally, after calculating the average $\langle I(t) \rangle$ for all of the triangle wave ramps, we eliminated any outlier values of $\langle I(t) \rangle$ by applying a median filter from the SciPy Python library with a window size of 1 second. This was done to eliminate large, transient current fluctuations due to, e.g., electroporation or any sharp discontinuities in the applied voltage occurring on the subsecond time scale. The processed values of C(t) can then be plotted against the processed voltage signal, as shown in Fig. 5(a) in the main text.